

PROCEEDINGS OF SPIE

[SPIDigitalLibrary.org/conference-proceedings-of-spie](https://spiedigitallibrary.org/conference-proceedings-of-spie)

Hybrid integration of laser source on silicon photonic integrated circuit for low-cost interferometry medical device

Matthieu Duperron, Lee Carroll, Marc Rensing, Sean Collins, Yan Zhao, et al.

Matthieu Duperron, Lee Carroll, Marc Rensing, Sean Collins, Yan Zhao, Yanlu Li, Roel Baets, Peter O'Brien, "Hybrid integration of laser source on silicon photonic integrated circuit for low-cost interferometry medical device," Proc. SPIE 10109, Optical Interconnects XVII, 1010915 (20 February 2017); doi: 10.1117/12.2250921

SPIE.

Event: SPIE OPTO, 2017, San Francisco, California, United States

Hybrid Integration of Laser Source on Silicon Photonic Integrated Circuit for low-cost Interferometry Medical Device

Matthieu Duperron^{a,*}, Lee Carroll^a, Marc Rensing^a, Sean Collins^a, Yan Zhao^a, Yanlu Li^b,
Roel Baets^b, Peter O'Brien^a

^aUniversity College Cork, Tyndall National Institute, Photonic Packaging Group, Dyke parade, Cork, Ireland

^bGhent University - IMEC, Photonics Research Group, iGent Tower - Department of Information Technology (INTEC) Technologiepark-Zwijnaarde 15, B-9052 Gent, Belgium

Abstract. The cost-effective integration of laser sources on Silicon Photonic Integrated Circuits (Si-PICs) is a key challenge to realizing the full potential of on-chip photonic solutions for telecommunication and medical applications. Hybrid integration can offer a route to high-yield solutions, using only known-good laser-chips, and simple free-space micro-optics to transport light from a discrete laser-diode to a grating-coupler on the Si-PIC. In this work, we describe a passively assembled micro-optical bench (MOB) for the hybrid integration of a 1550nm 20MHz linewidth laser-diode on a Si-PIC, developed for an on-chip interferometer based medical device. A dual-lens MOB design minimizes aberrations in the laser spot transported to the standard grating-coupler ($15\mu\text{m} \times 12\mu\text{m}$) on the Si-PIC, and facilitates the inclusion of a sub-millimeter latched-garnet optical-isolator. The 20dB suppression from the isolator helps ensure the high-frequency stability of the laser-diode, while the high thermal conductivity of the AlN submount ($300\text{W}/\text{m}\cdot^\circ\text{C}$), and the close integration of a micro-bead thermistor, ensure the stable and efficient thermo-electric cooling of the laser-diode, which helps minimise low-frequency drift during the approximately $\sim 15\text{s}$ of operation needed for the point-of-care measurement. The dual-lens MOB is compatible with cost-effective passively-aligned mass-production, and can be optimised for alternative PIC-based applications.

Keywords: optics, photonics, laser, hybrid integration, photonic packaging, micro-optical bench.

* matthieu.duperron@tyndall.ie

1 Introduction

Photonic Integrated Circuits (PICs) have emerged as a potential platform for a large number of information and communication technology (ICT), sensing, and medical applications, especially where high levels of integration are required. In particular, the development of Silicon-based PICs (Si-PICs) allows for integrated photonics and electronics with standard CMOS (Complementary Metal-Oxide-Semiconductor) processes, which can be very low-cost, when operated at high-volumes. The integration of coherent light sources on Si-PICs is a key challenge to unlocking the full potential of this platform. As an indirect-gap semiconductor, Si is a poor light emitter, and so recent efforts for source development on Si-PICs have focused on efficient and cost-effective ways to integrate direct-gap III-V materials and laser-dies on Si-PICs.

Heterogeneous integration involves bonding a piece of gain medium onto the Si-PIC, with evanescent coupling between this active material and the silicon waveguide. The laser cavity condition can be obtained by patterning the facets of the gain medium and/or by designing resonant structures on the Si-waveguides such as race-tracks and DBR (Distributed Bragg Reflector).¹ Heterogeneous integration technology is compatible with wafer-scale level processes, making it potentially cost-effective for numerous ICT applications, but it also has limitations, such as reduced customizability of the laser type. For example, in medtech applications there is sometimes the need for high power, e.g. multi-beam tissue scanning,² specifically high linewidth, e.g. interferometric

sensing,³ or broad wavelength range, e.g. Optical Coherence Tomography,⁴ and/or polarization control.⁵ Furthermore the wavelength of interest may vary usually in-between 600nm and 1000nm (biological window) but also in deeper infrared with applications at 1300nm⁴ and 1550nm.³ A platform capable of integrating a variety of known-good laser chips can accelerate the development of Si-PIC based technology for this broad range of measurements.

Hybrid integration of fully-processed laser chips allows for a high level of customizability, and can be implemented with either an edge-coupling or grating-coupling scheme.⁶ In the edge-coupling configuration, light is directly transferred horizontally from an edge-emitting laser-die to an edge-coupler on the Si-PIC waveguide. Mode adapters on the edge-coupler are usually used at the end of the waveguide to ensure high coupling efficiency and low back-reflections, and allows direct laser-to-PIC butt-coupling to be achieved.⁷ However, tight sub-micron alignment between the laser and PIC is required, and the chip should be fixed using reflow of solder bumps or thermo-compression bonding to minimize alignment drift,^{8,9} which can limit the vertical alignment. While edge-coupling hybrid integration allows low insertion-losses, and offers broadband coupling, it cannot be achieved at the wafer-level, because it requires chip-level processes such as facet polishing or etching, which ultimately increases the cost of the final device. In contrast, grating-couplers allow vertical integration that is compatible with wafer-level testing, and offer relatively efficient coupling ($< 3dB$ loss) and relaxed alignment tolerances ($\pm 5\mu m$ for $3dB$ loss).

Hybrid integration with VCSELs (Vertical-Cavity Surface-Emitting Lasers),¹⁰ and edge-emitting laser-diodes¹¹ is possible. For edge-emitting laser diodes, micro-optics (micro-lens and mirrors) are employed to steer and focus the laser beam, and have led to the concept of a Micro-Optical-Bench (MOB).¹² The micro-components on the MOB, including laser-diode, ball-lenses, steering-prism, and optical-isolator, can all be passively self-aligned on a finely-patterned sub-mount. The MOB is then actively aligned to the Si-PIC as a single unit, with a 2 axes-of-freedom, and fixed in place after the maximum coupling condition has been found. This integration approach is compatible with wafer-level mass-production, as shown by the product developed by Luxtera for high-speed interconnects,^{13,14} and is a promising route to cost-effective laser integration for Si-photonics.

In this paper, we describe the development of a MOB for the integration of a laser-die on a Si-PIC, as part of an on-chip 1550nm Doppler vibrometer for point-of-care arterial pulse wave velocity (PWV) measurements.¹⁵ This work is part of the H2020 European funded CARDIS¹⁶ project (Early stage CARDio Vascular Disease Detection with Integrated Silicon Photonics). For such Doppler measurement, the phase stability of the laser is critical, and so a sub-millimetric latched-garnet optical isolator with a $> 20dB$ isolation is included in the MOB, to reduce external feedback into the cavity. In addition, low-frequency drifts in the laser output are minimized by stabilizing the MOB temperature with thermo-electric cooling, and using a AlN ceramic sub-mount, which has a high thermal conductivity ($300W/m\cdot^{\circ}C$), to efficiently transfer heat from the laser-diode to the Si-PIC and into the bulk device. Section 1 describes the opto-mechanical design of the micro-optical bench with discrete latched-garnet isolator. The assembly process and the impact of alignment and assembly tolerances are presented in section 2. And section 3 presents and discusses the results of optical coupling.

2 Design

2.1 Optical Design

The integration of an isolator is needed for applications that require high stability of the laser output. The isolator ensures that reflections in the light path, at PIC or free-space level, are not back-coupled into the laser cavity, where they can lead to positive feedback that introduces high-frequency instability in the emission. Efficient on-chip-integrated isolators are not yet available,¹⁷ but the hybrid integration approach allows for the inclusion of a free-space-coupled isolator, using a sub-millimetric latched-garnet Faraday rotator.¹³ In this work, a fully-processed discrete isolator is used in the MOB to optimise the laser performance.

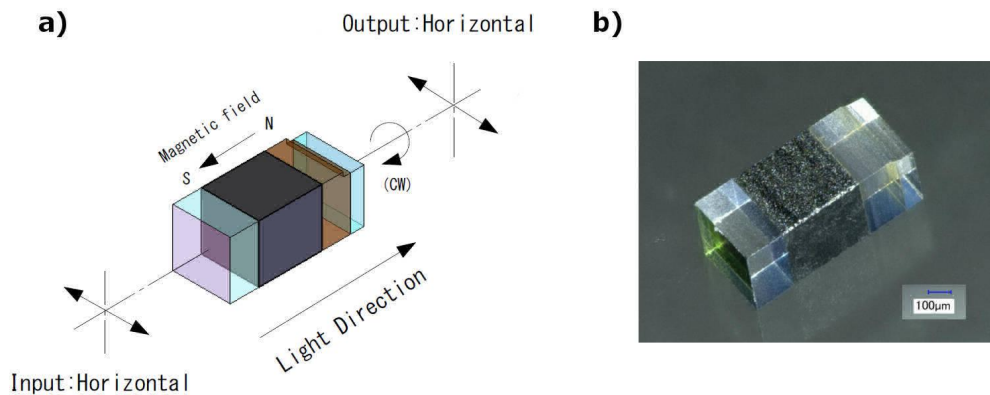


Fig 1 Isolator schematic (a) and picture (b)

The design of the isolator is presented figure 1. The horizontally polarized light of the laser travels first through a $200\mu\text{m}$ thick layer of glass, which is only added to protect the garnet from chipping during the dicing step in manufacture. Then a $440\mu\text{m}$ latched-garnet faraday rotator performs a 45° rotation of the polarisation. A $200\mu\text{m}$ 45° polarizer and a $90\mu\text{m}$ half-wave plate ensure the polarization filtering, and provide the horizontal polarization required for optical insertion into the standard TE (transverse electric) polarized grating coupler. Back reflections not filtered by the polarizer, i.e. horizontally polarized at the output of the isolator, will be rotated by the garnet into a vertical polarization that does not couple into output mode of the laser chip. This sub-millimetric isolator ($930\mu\text{m} \times 400\mu\text{m} \times 400\mu\text{m}$) is specified with a $> 20\text{dB}$ isolation performance for a clear aperture of $300\mu\text{m}$.

Compared to the previous MOB designs,^{12,13} the inclusion of this isolator introduces a relatively long additional optical path length ($930\mu\text{m}$ assumed in glass material BK7) between the laser and the Si-PIC, and this must be taken into account when making the lens design. In the following paragraph, different ball-lens systems for the MOB are investigated, using the Zemax software, with the requirement that the design be compatible with passive alignment, see section 2.2. The main purpose of the lens system is to image the laser-diode output onto the surface of the Si-PIC, while matching the imaged beam profile to the footprint of the grating coupler. In a first approximation, this can be seen as transforming the high numerical aperture (NA) of the laser

output (0.19 in horizontal direction X and 0.25 in vertical direction Y) into a lower NA (0.095 for both directions). In this work, a standard TE-polarized grating coupler, optimized for butt-coupling of a SMF-28e fiber with a $10.4\mu\text{m}$ mode-field-diameter (MFD) is used.

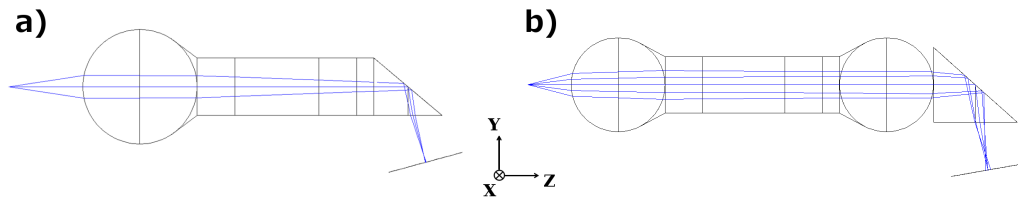


Fig 2 a) 1 lens design with a $800\mu\text{m}$ diameter sapphire Ball lens; b) 2 lenses design with $500\mu\text{m}$ diameter lenses (sapphire and BK7)

The figure 2 a) presents such an optical system with a $800\mu\text{m}$ diameter sapphire ball lens ensuring numerical aperture matching. The ball lens is in contact with the isolator, the gap is filled with epoxy (index 1.55) in order to decrease the focal length of the system. A $300\mu\text{m}$ -high prism in direct contact with the isolator redirects the light with a 10° angle optimized for the grating coupling. The distance between the bottom of the prism and the grating coupler is fixed at $254\mu\text{m}$ for manufacturing reasons. In this configuration the path length between the lens and the grating coupler is minimized.

The figure 3 a) presents the coupling efficiencies into a standard fiber for different ball-lens diameters and materials (BK7 $n=1.52$, Sapphire $n=1.77$, LaSf35= 2.02) computed with the Physical Optics Propagation toolbox of Zemax. The total coupling efficiency is the product of the fiber mode matching (continuous lines) with the system efficiency (dashed lines), which represents the effect of the losses due to the surface reflections and the limited diameter of the optical components. For each simulated system, the laser to ball-lens system has been optimized to maximize the fiber mode matching, see figure 3 b). Here, to ensure the computational convergence of the Zemax simulations, the numerical aperture of the gaussian beam of the laser is fixed at 0.115 in X and 0.15 in Y. As a first-order approximation in these simulations, the acceptance of the grating coupler is assumed to behave similarly to a SMF-28e fiber. For the three materials, the fiber mode matching increases with lens diameter, and with a decrease in the refractive index of the lens for lens diameters $< 750\mu\text{m}$, both of which correspond to an increase in the focal length of the MOB. Note that in this system, the distance between the lens and the output coupler is fixed by the isolator/prism/mount dimensions, so when the focal length of the lens is increased, the laser to ball-lens distance is simultaneously increased to achieve focus on the coupler plan (figure 3 b). This creates a higher numerical aperture beam after the lens, and hence a smaller beam size on the output coupler. This increase of focal length is nevertheless limited by practical effects. Firstly, for integration purposes, it is not desirable to use ball lens that are bigger than $800\mu\text{m}$ (because the size of the MOB becomes too large), so it is not possible to reach the optimized NA conversion, even with BK7 lenses. Secondly, the clear aperture of the isolator ($300\mu\text{m}$ diameter) gives an upper limit on the MFD of the beam after the lens, as shown by the decrease of system efficiency for the BK7 ball lens with diameter greater than $700\mu\text{m}$. Thirdly, using low-index ball-lenses with high aperture introduces a large spherical aberration, as shown in figure 3 c) for BK7 material. These

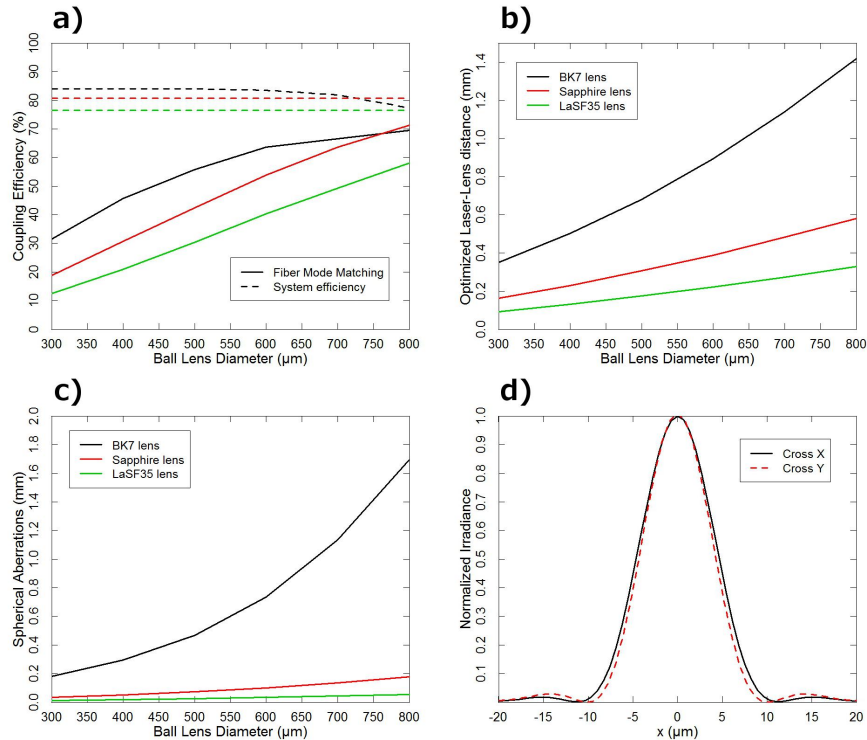


Fig 3 a) Coupling Efficiency for different ball lens diameters separated between fiber mode matching efficiency (lines) and system efficiency (dashed lines) for BK7 (black), Sapphire (red) and LaSF35 (green) ball lenses; b) Optimized laser to lens distance; c) Spherical aberrations computed for a NA of 0.15; d) Cross-X and Cross-Y of the beam profile for a $800\mu\text{m}$ diameter BK7 ball lens exhibiting large spherical aberration (1.7mm in Y and 0.6mm in X for laser NA 0.115 in X and 0.15 in Y)

aberrations introduce high-order amplitude and phase components in the nominally Gaussian spot imaged onto the grating-coupler of the SI-PIC, see figure 3 d) with the appearance of side lobes on the irradiance profile. This reduces the mode-matching between the grating-coupler and imaged spot, and increases the insertion-loss, which can be seen in figure 3 a) with the curve inversion of the fiber mode matching for BK7 (black curve).

To overcome these difficulties, and optimally couple light from laser to grating coupler with a long path length due to the isolator, a two-lenses design is proposed. The first lens collimates the beam from the laser, and the second focus the beam on the grating-coupler with the optimized NA. The distance between the two lenses can be tuned depending on the requirement as the beam is collimated. Here the $930\mu\text{m}$ thick isolator is introduced as seen in figure 2 b). The collimation quality (Rayleigh range) required for such an isolator length can easily be achieved with micro-ball-lenses.

The use of two lenses allows drastically reduced spherical aberrations because of the split of refractive power over 4 curved surfaces, and the use of a collimated configuration.¹⁸ Unfortunately, it also increases the surface reflection losses and tightens the misalignment tolerances of the lenses due to the relatively small corresponding front focal length. As a compromised solution, adding an index-matching epoxy (refractive index 1.55) between the lenses and the isolator significantly

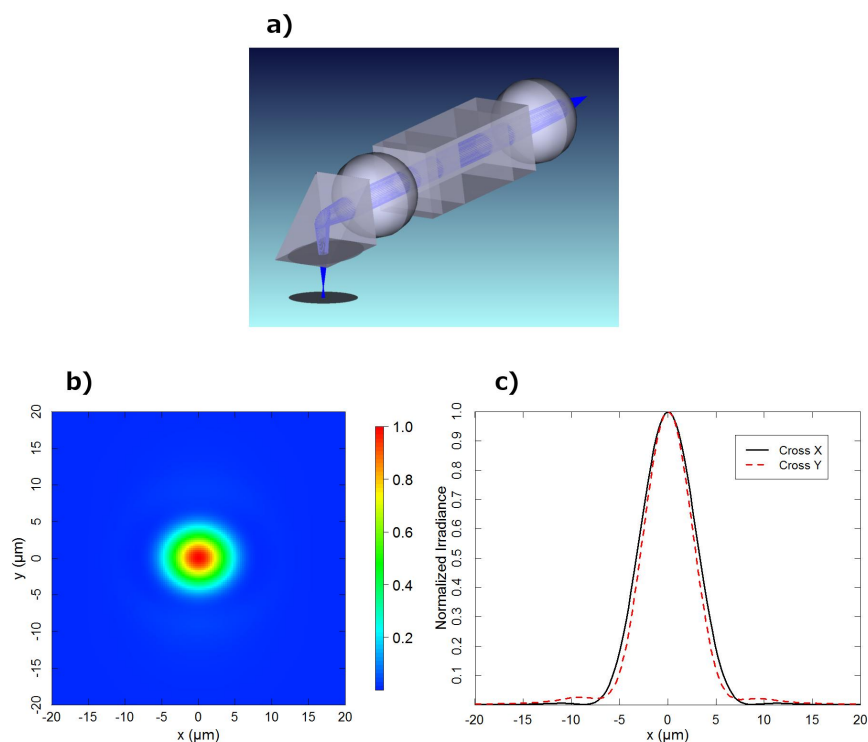


Fig 4 a) 3D view of the optical design (epoxy between the ball lenses and the isolator not represented); b) 2D beam profile of the focusing point at the grating coupler position, normalized intensity; c) Cross-X (black curve) and Cross-Y (red dashed curve) of the beam profile

reduces the reflection losses, without altering the coupling performance, because the spherical aberration remains low. The proposed design is plotted in figure 2 b) and figure 4 a). This design incorporates a sapphire $500\mu\text{m}$ diameter ball-lens (first lens) placed $230\mu\text{m}$ from the laser edge, the isolator, a BK7 $500\mu\text{m}$ diameter ball-lens (second lens) and a $400\mu\text{m}$ prism with angles $41, 7^\circ$ and $48, 3^\circ$ in order to steer the beam at 10° from the vertical axis. For a laser beam of $NA_X = 0.115$ and $NA_Y = 0.150$, this MOB design reaches an optimal Fiber Mode Matching of 96% and an overall System transfer efficiency of 75%. Spherical aberrations remains low in this configuration, with 0.033mm in X and 0.096mm in Y. The use of a two-lens design adds another advantage: the light traveling through the isolator is now collimated allowing optimise isolation performance.

Any increase in the NA of the laser-diode directly scales to an increase of the MOB output NA, hence a smallest beam-spot on the grating coupler and increased spherical aberration, altering the performance of the coupling. Typically for a NA_X of 0.19 and a NA_Y of 0.25 from the laser diode, the fiber mode matching drops to 77%, and the spherical aberration increases to 0.843mm in Y and 0.259 in X. In this configuration side lobes on the beam spot can be seen in the Y direction, figure 4 b) and c).

2.2 Mechanical Design

In this second design section, the manufacturability of such optical system with passive alignment using a patterned ceramic mount is evaluated. The first part describes the alignment tolerances of the optical design and the second part presents the ceramic design.

The misalignment tolerances for the coupling to a standard fiber are presented table 1. The most critical alignment, i.e. the centering of the first ball lens, allows for 1dB loss, out-of-axis misalignments in the horizontal direction (X) of $12\mu m$ and in the vertical direction (Y) of $11\mu m$ decentering. All the alignment tolerances appear to be relatively relaxed and achievable with passive mechanical alignment, as will be discussed in section 3. Furthermore, even if large misalignments in X and Y are encountered, they can be partially compensated during the active alignment of the MOB on the Si-PIC through a tilting correction, albeit at the cost of a longer alignment process that increases the degrees of freedom from the original 2 to 4. The axial misalignments, laser to first-lens distance and second-lens to prism distance, are more critical because they modify the position of the focusing plane, which cannot be easily recovered through re-positioning of the MOB. The decentering and tilting misalignment tolerances of the isolator and the prism (not presented here) are sufficiently relaxed that they can be achieved by manual alignment under a microscope.

Table 1 Misalignment tolerances for 1dB losses

Misalignment	1dB Tolerance
Laser Decenter X	$\pm 17\mu m$
Laser Tilt Y	$\pm 5^\circ$
Laser Decenter Y	$\pm 15\mu m$
Laser Tilt X	$\pm 4^\circ$
Lens 1 Decenter X	$\pm 12\mu m$
Lens 1 Decenter Y	$\pm 11\mu m$
Lens 2 Decenter X	$> \pm 30\mu m$
Lens 2 Decenter Y	$> \pm 30\mu m$
Laser - Lens1 distance	$\pm 15\mu m$
Lens 2 - Prism distance	$0 - 60\mu m$

The values presented in table 1 correspond to the coupling between the MOB and a standard single mode fiber ($MFD = 10.4\mu m$), as a good analogue to the acceptance footprint of a grating coupler. Of course some small variations may be expected for the coupling to a grating coupler designed to match such fiber. It is worth noticing, that vertical (Y) misalignments will mainly result in a variation of the angle of the beam out of the targeted 10° , hence a shift of the optimal wavelength of the coupling.

In order to achieve such tolerances with a passive alignment of the different optical components, an AlN ceramic mount has been designed, see figure 5. This $1.6mm \times 3.3mm \times 0.254mm$ ceramic is patterned to aid in the mechanical positioning of the two lenses. A $300\mu m$ -wide trench

is laser-drilled to align the ball-lenses and position their center at a height of $200\mu\text{m}$ of the ceramic surface. This trench allows alignment of the two ball-lenses compared to the other features of the ceramic without adding the misalignment that would appear by patterning two holes centered with a $\pm 20\mu\text{m}$ position tolerance. Furthermore the trench will be used to visually align the other components: laser die, isolator and prism. The $\pm 30\mu\text{m}$ tolerance specified for the fabrication of the wideness of the trench results in a $-12/+10\mu\text{m}$ position of the lens which is in the 1dB loss range, see table 1. The vertical alignment of the isolator and prism is obtained by lying them directly on the pad ceramic. The vertical alignment of the laser is obtained by lying it on a metallic pad. Using $100\mu\text{m}$ thick laser chip, the $500\mu\text{m} \times 500\mu\text{m}$ metallic pad has to be high of $100\mu\text{m}$. A thick gold layer ($95\mu\text{m}$) has been electroplated and a finishing $5.2\mu\text{m}$ AuSn layer is evaporated for further solder reflow to fix the laser chip. This thick pad approach enables the integration of most of the off-the-shelf fully-processed laser dies as it allows compensating for their different thicknesses. A laser-drilled alignment mark between the trench and the metallic pad is added for lateral alignment of the laser.

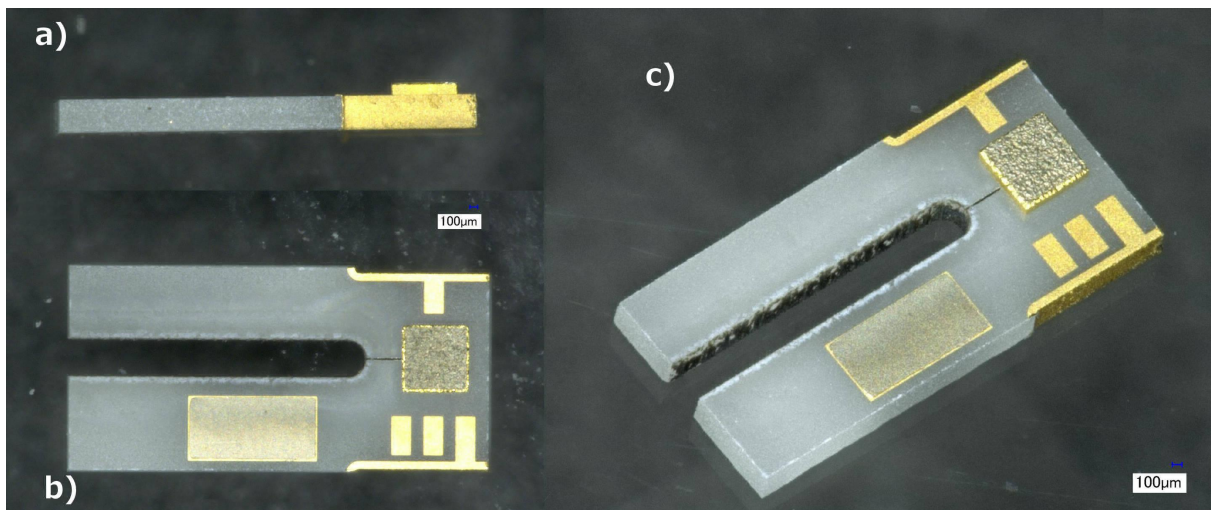


Fig 5 a) side view, b) top view and c) angled view of the ceramic bench

Other features have been designed to optimize the assembly process and the ultimate performances. Side contacts are connected to top contacts for connection through wire-bonds to the laser. Using a specially designed gripping tool with electrically conductive levers, the side contacts allow powering of the laser during the alignment without connecting extra wires, simplifying handling during the active alignment on the Si-PIC. An additional metallic pad is added to the MOB to allow for the surface mounting of a $300\mu\text{m} \times 300\mu\text{m}$ thermistor, to measure the temperature of the laser chip for feedback to the thermo-electric cooling.

2.3 Thermal Design

The last topic of the design concerns the thermal management. The micro-optical-bench is made of AlN ceramics for its high thermal conductivity ($300\text{W}/\text{m}\cdot^\circ\text{C}$). The heat evolved by the laser to

provide at least 2.5mW of CW-optical power in the Si-waveguide is estimated at 90mW . This rate of heat flow into the MOB can easily be managed by an off-the-shelf Peltier element.

The temperature of the laser and of the PIC are measured with thermistors respectively on the MOB and on the mount of the PIC. The motivation for adding the thermistor on the MOB is to measure the temperature of the laser as accurately as possible, by avoiding significant thermal load between the laser and the sensor. For this purpose, the choice of thermally conductive AlN ceramic should allow accurate measurement avoiding any temperature drift of the laser.¹⁹ Furthermore, direct knowledge of the absolute value of the laser temperature allows optimal wavelength tuning of the light, knowing that the temperature tuning coefficient of the laser is typically $0.1\text{nm}/^\circ\text{C}$.

3 Assembly

The first component to be assembled on the ceramic bench is the laser chip because of the heating required for reflow the AuSn solder layer. Standard flip-chip techniques are used and as previously mentioned, it is vertically aligned with respect to the metallic pad design. The first horizontal alignment is made by using the trench sides to compensate for any tilting. Then the axial position is set at $330\mu\text{m}$ from the end of the trench, using the manual translational stage of the flip-chip machine, see figure 6 a). Its horizontal centering is optimized in regards to the alignment mark, although this process is made somewhat difficult by the combined thicknesses of the laser chip and pad ($100\mu\text{m}$ each) which exceeds the depth of focus of the microscope, and so requires an adjustment to the zoom and focus of the microscope to view both the laser waveguide and the alignment mark on the AlN ceramic. A reproducibility of $\pm 5\mu\text{m}$ and $\pm 1^\circ$ in laser-die position can be expected from this alignment protocol. The AuSn layer is reflow at 340°C during 20s and a 1 to 5N pressure is applied on the laser chip for thermo-compression.

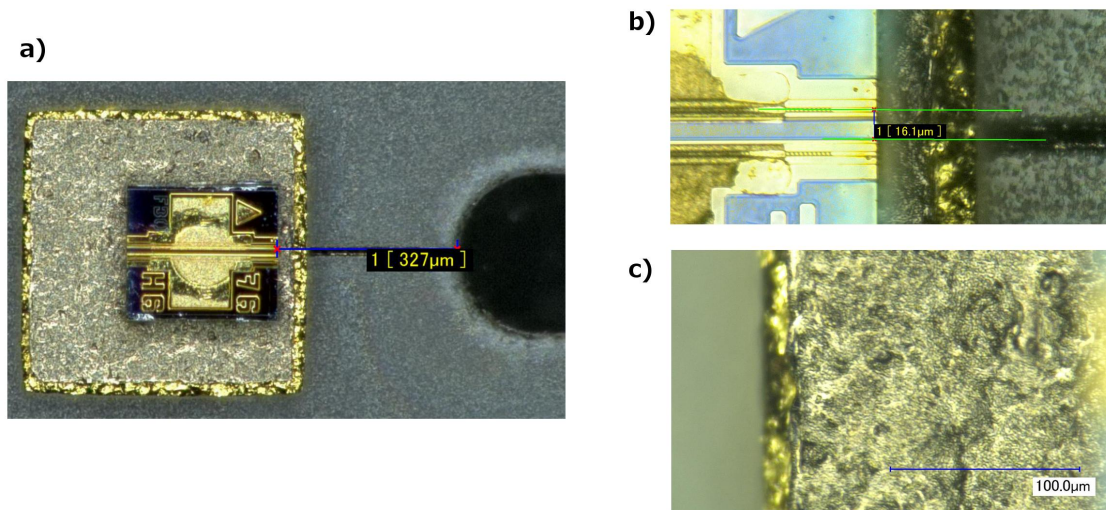


Fig 6 a) Visual alignment of the laser chip using standard flip-chip techniques to align the laser ridge with the alignment mark; b) Decentering measured after solder reflow; c) AuSn and Au surface roughness

During the reflow process, the laser chip has a tendency to shift from its initial position, as shown on figure 6 b) where, after bonding, a $16\mu\text{m}$ shift of lateral position was measured. This unexpected behavior is probably due to the roughness of the metallic pad on which the die is bonded, and will be addressed in future versions of the MOB. The figure 6 c) shows the significant roughness present on the top surface of the $95\mu\text{m}$ -thick Au layer and $5\mu\text{m}$ -thick Ausn layer. High thermocompression forces of 5N seem to decrease these lateral shifts. Despite this effect, a horizontal alignment accuracy of $\pm 15\mu\text{m}$ and $\pm 5^\circ$ can be expected.

The vertical alignment of the chip is accurate with a $\pm 10\mu\text{m}$, where the uncertainty is mainly due to the variation of Au pad thicknesses obtained during electroplating. A $\pm 3\mu\text{m}$ accuracy can be obtained by sorting-and-binning the best ceramics.

The optical components are manually positioned and fixed on the trench, one after the other, in order that light passes through them. High viscosity UV-curable epoxy ($57,500\text{ cP}$) is used to make micro-drops of approximately 1 nL . The viscosity and size of the drops allow for strong bonding of the different components, and the surface tension helps avoid the spreading of epoxy over the optical surfaces.

The first ball-lens is mechanically positioned in the trench after a micro-drop has been dispensed. Epoxy is then applied to the surface of the isolator, before being pushed into contact with the lens, and aligned with respect to the trench. Similarly, epoxy is dispensed on the output facet of the isolator, before the second ball-lens is mechanically positioned in contact with it, using the trench for alignment. Finally, the prism is positioned in contact with the second lens, and aligned with the trench, then glued on its side with the ceramic. The figure 7 shows a fully assembled micro-optical bench. This passive alignment protocol allows all components to be aligned within the specifications defined previously, see section 2.2, and so is a route to cost-effective assembly of the MOB.

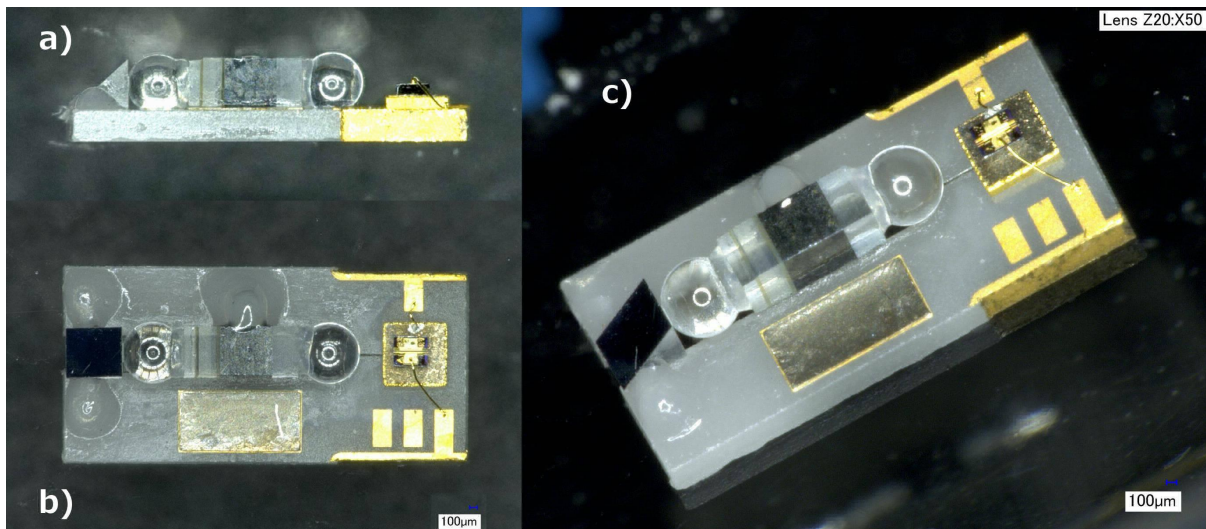


Fig 7 a) side view, b) top view and c) angled view of the Micro-optical bench, without thermistor

4 Results and discussion

4.1 Beam characterization

In order to qualify the quality of the alignment, the beam profile at the focusing point is measured.²⁰ A lensed-fiber, SMF-28e with a tip angle of $85 \pm 5^\circ$ and a radius of $11 \pm 1\mu m$, is used to scan the light beam in the focal plan of the MOB with a step of $0.5\mu m$. To minimize heating effects, the laser-diode in the MOB is powered by a pulsed power-supply at $3.5kHz$, and a fill-factor of $\sim 40\%$ to a maximum current of $44mA$. The optical signal coupled to the fiber is measured by an InGaAs sensor with an integration time much larger than the pulsed period, to provide good averaging. The raw data of the measurement are interpolated on a $0.25\mu m$ grid. The lensed-fiber has an expected mode-field-diameter of approximately $3\mu m$. Here, we assume that the phase profile of the MOB beam is not changing rapidly, and can be considered as constant over the entire surface of the lensed-fiber mode profile, and so the power measured from coupling to the lensed-fiber corresponds linearly to the local intensity of the beam.

To deconvolve the effect of the measurement spot, the near-field of a cleaved SMF-28e fiber is measured in the same configuration. The measured profile is assumed to be the convolution of the lensed-fiber mode with a perfect Gaussian profile of diameter $10.4\mu m$. The measurement from the MOB is then deconvolved in Fourier space in order to extract the true MOB beam profile from the experimental data:

$$\mathcal{F}\{MOB_{deconv}\} = \frac{\mathcal{F}\{MOB_{measured}\} \times \mathcal{F}\{Gaussian\}}{\mathcal{F}\{Fiber_{measured}\}} \quad (1)$$

where $MOB_{measured}$ is the 2D scan measurement of the MOB beam profile, $Fiber_{measured}$ is the 2D scan measurement of the fiber beam profile, $Gaussian$ is the ideal Gaussian profile of the fiber and MOB_{deconv} is the final deconvolved profile.

The figure 8 presents the beam profiles for two different MOB. Figures 8 a) and b) correspond to a MOB with an alignment of the laser in the specification of table 1 while figures 8 c) and d) correspond to the beam profile of a MOB for which the laser position is laterally shifted of approximately $30\mu m$.

The spot diameters measured for the aligned MOB (fig 8 a and b) are $15\mu m$ in X and $14\mu m$ in Y for the $1/e^2$ value of a fitted gaussian profile. The profiles exhibit a good fit to a Gaussian curve with low side lobes, which confirms the low level of aberrations in the beam. These results are in relatively good agreement with the design in which relatively smaller diameter have been observed: $11\mu m$ and $10\mu m$ diameter in X and Y respectively (see figure 4). This could be explained by a too great distance between the laser and the first ball lens compared to the ideal design, resulting in a change of NA and beam size. Indeed this would increase the beam diameter at focus and shortened the distance between the prism and the focal point. This last point has also been observed during the measurement that identified the focal plane (defined as the plane in which the spot has maximum intensity) as being located slightly inside the ceramic ($\sim 10 - 20\mu m$).

The misaligned MOB, figures 8 c) and d), shows a very disturbed profile indicative of strong aberrations. The beam spot is bigger and the focal point was found deep into the ceramic ($\sim 100\mu m$) which proves once again the presence of a strong defocus probably due to a large laser-lens distance. The diameter of the beam spot is 40% bigger in X axis than in Y axis. This strong

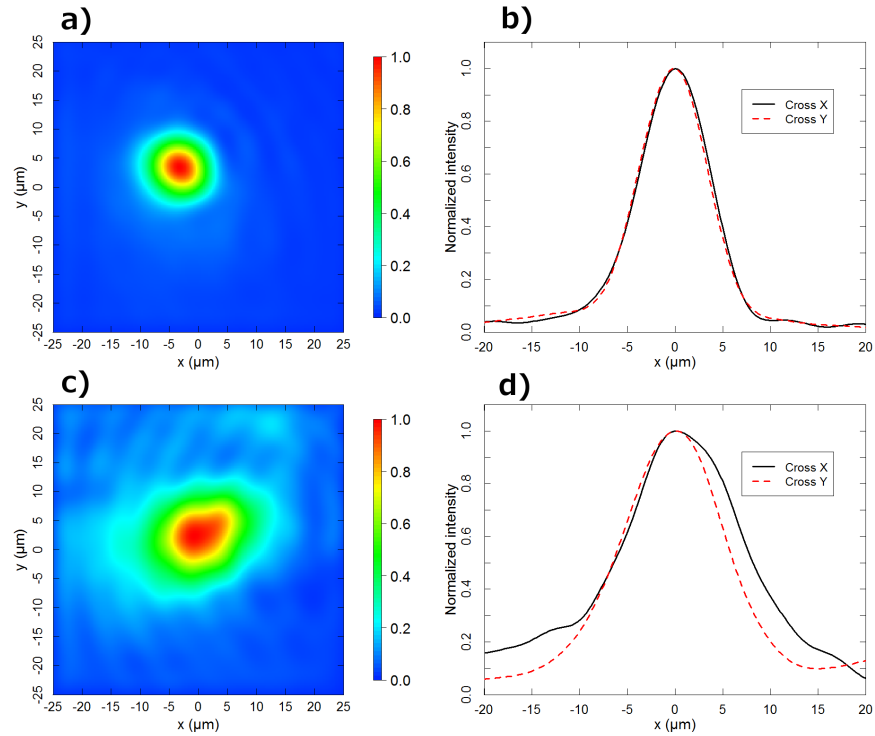


Fig 8 a) and b) Deconvolved beam spot of an aligned Micro-Optical Bench measured with a $3\mu\text{m}$ -MFD lensed fiber, a) 2D scan (normalized intensity), b) cross X and Y; c) and d) similar plots for a MOB with a laterally misaligned laser chip

astigmatism is due to the lateral misalignment of the laser measured at more than $30\mu\text{m}$ which also shift the measured focus point of approximately $50\mu\text{m}$ laterally compared to the centered design. Finally, ripples are observable in the X direction. These can be explained as originating from diffraction effects, most likely originating from the edge of the isolator. If the beam is significantly decentered and out-of-focus, then the clear aperture of the isolator may not be big enough to accommodate the beam, and light from the collimated beam will be diffracted by the edge.

The study of the focused beam profiles gives a good indication of the quality of the underlying alignment. The presence of astigmatism and defocus in the beam are indicative of lateral and axial alignment of the laser chip on the MOB.

4.2 Alignment on PIC and performances

The MOB is actively aligned on a standard "building block" 1550nm grating-coupler from the IMEC Si-Photonic MPW service. A mechanical gripper is used to hold the MOB during the alignment and to power the laser through the levers in contact with the metallic side-contacts of the ceramic, see figure 9. This allows simple manipulation of the MOB with a standard alignment machine for sub-micron alignment.

Only the displacements in plan (X and Y) require active alignment. All the other axes are pre-aligned by gripping the MOB on a flat surface and visually adjusting yaw angle and vertical

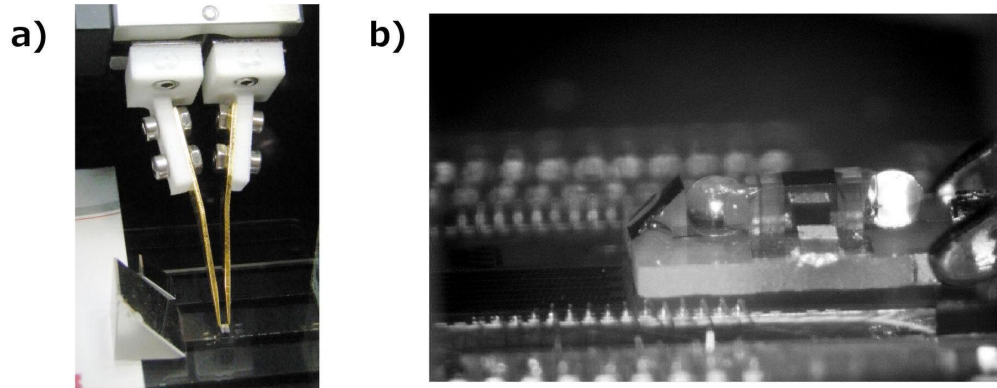


Fig 9 a) Electrically powered mechanical gripper holding a micro-optical bench. b) Micro-optical bench aligned on PIC using the developed gripper tool.

direction. This 2-axes-of-freedom in the active alignment simplifies the process allowing it to become relatively cost-effective when scaled to the wafer level. The variation of light coupling with the horizontal displacements is plotted figure 10. The scan range in X is limited to $-5\mu\text{m}$ to ensure the wirebonds on the chip are not impacted.

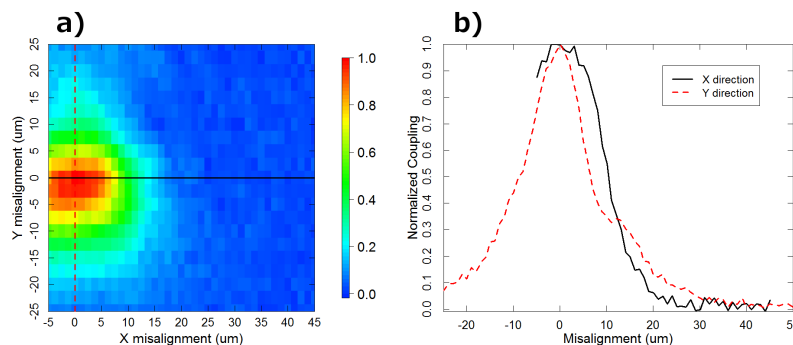


Fig 10 Normalized coupling efficiency through a standard grating coupler a) 2D map of X and Y misalignments, b) cross X and cross Y plots.

The measured alignment tolerances appear to be more relaxed than predicated by simulations, with a 50% coupling (3dB losses) at $\pm 11\mu\text{m}$ in X and $\pm 8\mu\text{m}$ in Y for $\pm 5\mu\text{m}$ expected. This is due to the larger beam spot in the real samples, compared to the ideal design, and is enhanced by a small distance between the ceramic and the PIC during the alignment, making the unfocused beam spot approximately twice larger than expected on the grating than expected.

The figure 11 shows the spectrum of the light coupled in the PIC. The light in the PIC is measured via a fiber coupled to a grating coupler on the PIC and connected to an Anritsu MS9710c optical spectrum analyser. The frequency of the pulse of the power-supply of the laser is slowed down to 12Hz and its fill factor increased in order to ensure a CW-laser power during the sweeping measurement of the spectrum analyzer and to control the thermal heating. Two different fill-factors have been tested: 50% and 90%.

In order to normalize the measured value, the similar device has been measured with a standard cleaved fiber (SMF-28e) instead of the MOB and a broadband SLD. This gives a reference value for a standard coupling performance. To remove the effect of the losses in the PIC and in the measurement system, the measured MOB spectrum has been divided by the reference measurement following the equation:

$$Losses = \frac{MOB_{spectrum} / Laser Power}{Fiber_{spectrum} / SLD_{spectrum}} \quad (2)$$

where $MOB_{spectrum}$ is the spectral measurement of the MOB-PIC assembly, $Laser Power$ is the power from the laser chip, here $10.7mW$ with a current of $44mA$, $Fiber_{power}$ is the spectrum of the fiber-PIC assembly and is normalized by the SLD spectrum $SLD_{spectrum}$. The resulting $Losses$ correspond to the integration penalty of the MOB compare to a standard fiber, i.e. the mismatching of the beam profile and the surface reflections introduced by the MOB.

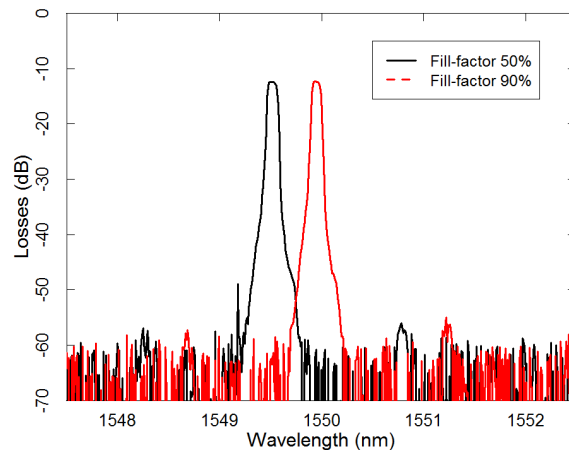


Fig 11 Spectrum of the laser coupling to the grating coupler for different fill-factor of the laser pulsed power supply with a 12Hz frequency to ensure CW measurement during the sweeping of the spectrum analyzer.

A $12dB$ losses is observed. This value is significantly high compare to the $3dB$ expected from design and is to be put into perspective: an off-the-shelve package would have a $4 - 5dB$ losses for coupling the laser light to a fiber. Those $12dB$ losses are partially resulting from the defocus of the optical system and could be optimized with better adjustment of the laser position and of the vertical alignment of the MOB during the alignment on the PIC. An estimated $2 - 3dB$ can be recovered with a better focus. Surface reflections plays a significant role with $1.25dB$ losses expected from the design. But more reflections are appearing because of the anti-reflective coatings on the isolator facets. Those coatings have been optimized for air/glass interface but are not needed for this MOB design with the matching-index epoxy on the isolator facets. The resulting increase of losses hasn't yet been quantified.

The spectrums of figure 11 show the expected discrete laser mode, used for the interference-based sensing application. The observed linewidth is to be discussed with care as the resolution of the Spectrum Analyser is $0.1nm$ and is too large to measure linewidth around $20MHz$. Nevertheless, it seems the observed spectral linewidth is significantly large. This is the result of the

noisy signal driving the laser current from the pulse generator which introduces high frequency instability in the measurement. Finally, a variation of wavelength of 0.45nm appears when changing the fill-factor of the power-supply from 50% to 90%. A change of duty cycle results in a change of heat from the laser to be dissipated only by the pick-up tool as no cooling system is set up. For important fill-factors, the heat hasn't enough time to be dissipated resulting in an increase of the temperature of the MOB. From the specification of the laser, a temperature tuning coefficient of $0.1\text{nm}/^\circ\text{C}$ is expected, this correspond to an increase of temperature of approximately 4.5°C . No amplitude variation are observed in this 0.45nm range, which is expected as the free-space coupling system is broad band.

5 Conclusion

We have assembled and validated a two ball-lens micro-optical bench, with a sub-millimetric integrated optical isolator and a 1550nm 20Mhz linewidth laser diode, designed for simplified active alignment on Si-PICs (both at die- and wafer level). The two ball-lens design allows for the easy insertion of the discrete latched-garnet isolator, while minimizing optical aberrations through the MOB, preserving the planar wavefront of the laser beam at the grating-coupler, and so maximizing the coupling efficiency. The combination of relaxed alignment tolerances of the optical design, alignment patterns and alignment trench engineered into the AlN ceramic sub-mount of the MOB, allows for the passive and self-alignment of the laser-die, the ball-lenses, the isolator and the turning-prism on the MOB. This supports fast, low-cost, and scalable assembly of the MOB, and is complimented by the electrical design of the MOB which allows "powered tweezers" to both mechanically position and electrically drive the MOB during active alignment to a Si-PIC. The performance of the two ball-lens MOB is mainly limited by the lateral and axial placement of the laser chip on the MOB which is non-trivial because of the surface roughness introduced by the $100\mu\text{m}$ thick Au pad deposited on the ceramic. Despite those misalignments, the alignment of the MOB on the PIC can be performed using only 2 degrees-of-freedom during active alignment, which allows for fast assembly times. MOB to PIC coupling to a standard "building block" 1550nm grating-coupler adds a 12dB penalty loss, compared to the measured Fibre-to-PIC insertion-loss. Simulations used to reconstruct the measured beam-profiles show where several design and alignment improvements can be made, to reduce the insertion-loss to 3dB, and these are now being pursued.

The MOB design developed in this work can easily be extended to accept most off-the-shelf laser dies, and so can be used as an integration-platform for many different applications that require low-cost hybrid integration of laser-sources on Si-PICs.

Acknowledgments

The work presented in this article is part of CARDIS project (Early stage CARDio Vascular Disease Detection with Integrated Silicon Photonics). This project has received funding from the European Union's Horizon 2020 Research and Innovation Program under grant agreement No 644798. The authors would like to thank Cicor Reinhardt Microtech AG for the fabrication of the AlN ceramic and the development of thick Au pad deposition for the purpose of this work.

References

- 1 B. Ben Bakir, C. Sciancalepore, A. Descos, H. Duprez, D. Bordel, L. Sanchez, C. Jany, K. Hassan, P. Brianceau, V. Carron, and S. Menezo, "Heterogeneously Integrated III-V on Silicon Lasers," in *SEMICONDUCTOR WAFER BONDING 13: SCIENCE, TECHNOLOGY, AND APPLICATIONS*, Moriceau, H and Baumgart, H and Goorsky, MS and Hobart, KD and Knechtel, R and Suga, T and Tan, CS, Ed., *ECS Transactions* **64**(5), 211–223, Electrochim Soc, Elect & Photon Div; Electro Vis Grp; X FAB Semiconductor Foundries AG; Appl Microengineering Ltd (2014). 13th International Symposium on Semiconductor Wafer Bonding - Science, Technology and Applications as part of the 226th Meeting of the Electrochem Soc, Cancun, MEXICO, OCT 05-09, 2014.
- 2 D. Culemann, A. Knuettel, and E. Voges, "Integrated optical sensor in glass for optical coherence tomography (oct)," *IEEE Journal of Selected Topics in Quantum Electronics* **6**(5), 730–734 (2000).
- 3 Y. Li, P. Segers, J. Dirckx, and R. Baets, "On-chip laser doppler vibrometer for arterial pulse wave velocity measurement," *Biomedical optics express* **4**(7), 1229–1235 (2013).
- 4 B. I. Akca, J. Kalkman, N. Ismail, G. Sengo, F. Sun, A. Driessen, T. G. van Leeuwen, M. Pollnau, K. Wörhoff, R. M. de Ridder, *et al.*, "Toward spectral-domain optical coherence tomography on a chip," *IEEE journal of selected topics in quantum electronics* **18**(3), 1223–1233 (2012).
- 5 G. Yurtsever, B. Považay, A. Alex, B. Zabihian, W. Drexler, and R. Baets, "Photonic integrated mach-zehnder interferometer with an on-chip reference arm for optical coherence tomography," *Biomedical optics express* **5**(4), 1050–1061 (2014).
- 6 C. Kopp, S. Bernabe, B. B. Bakir, J.-M. Fedeli, R. Orobtcchouk, F. Schrank, H. Porte, L. Zimmermann, and T. Tekin, "Silicon photonic circuits: on-cmos integration, fiber optical coupling, and packaging," *IEEE Journal of Selected Topics in Quantum Electronics* **17**(3), 498–509 (2011).
- 7 B. B. Bakir, A. V. de Gyves, R. Orobtcchouk, P. Lyan, C. Porzier, A. Roman, and J. Fedeli, "Low-loss (≤ 1 db) and polarization-insensitive edge fiber couplers fabricated on 200-mm silicon-on-insulator wafers," *IEEE Photon. Technol. Lett* **22**(11), 739–741 (2010).
- 8 T. Shimizu, N. Hatori, M. Okano, M. Ishizaka, Y. Urino, T. Yamamoto, M. Mori, T. Nakamura, and Y. Arakawa, "Multichannel and high-density hybrid integrated light source with a laser diode array on a silicon optical waveguide platform for interchip optical interconnection," *Photonics Research* **2**(3), A19–A24 (2014).
- 9 M. Kapulainen, S. Ylinen, T. Aalto, M. Harjanne, K. Solehmainen, J. Ollila, and V. Vilokkinen, "Hybrid integration of inp lasers with soi waveguides using thermocompression bonding," in *2008 5th IEEE International Conference on Group IV Photonics*, (2008).
- 10 H. Lu, J. S. Lee, C. Scarcella, Y. Zhao, P. Cardile, A. Daly, M. Ortsiefer, L. Carroll, and P. O'Brien, "Flip-chip integration of tilted vcsels onto a silicon photonic integrated circuit," *OPTICS EXPRESS* (2016).
- 11 A. Narasimha, B. Analui, E. Balmater, A. Clark, T. Gal, D. Guckenberger, S. Gutierrez, M. Harrison, R. Koumans, D. Kucharski, *et al.*, "A 40-gb/s qsfm optoelectronic transceiver in a

- 0.13 μm cmos silicon-on-insulator technology,” in *Optical Fiber Communication Conference, OMK7*, Optical Society of America (2008).
- 12 B. Snyder, B. Corbett, and P. O'Brien, “Hybrid integration of the wavelength-tunable laser with a silicon photonic integrated circuit,” *Journal of Lightwave Technology* **31**(24), 3934–3942 (2013).
 - 13 P. De Dobbelaere, G. Armijo, J. Balardeta, B. Chase, Y. Chi, A. Dahl, Y. De Koninck, S. Denton, M. Eker, S. Fathpour, *et al.*, “Silicon-photonics-based optical transceivers for high-speed interconnect applications,” in *SPIE OPTO*, 977503–977503, International Society for Optics and Photonics (2016).
 - 14 M. Mack, M. Peterson, S. Gloeckner, A. Narasimha, R. Koumans, and P. De Dobbelaere, “Method and system for a light source assembly supporting direct coupling to an integrated circuit,” (2012). US Patent 8,168,939.
 - 15 Y. Li and R. Baets, “Homodyne laser doppler vibrometer on silicon-on-insulator with integrated 90 degree optical hybrids,” *Opt. Express* **21**, 13342–13350 (2013).
 - 16 “CARDIS: early stage CARDio vascular disease Detection with Integrated Silicon photonics.” <http://www.cardis-h2020.eu>.
 - 17 L. Bi, J. Hu, P. Jiang, D. H. Kim, G. F. Dionne, L. C. Kimerling, and C. Ross, “On-chip optical isolation in monolithically integrated non-reciprocal optical resonators,” *Nature Photonics* **5**(12), 758–762 (2011).
 - 18 A. Siegman, “Analysis of laser beam quality degradation caused by quartic phase aberrations,” *Applied optics* **32**(30), 5893–5901 (1993).
 - 19 C. Eason, M. Rensing, J. S. Lee, and P. O'Brien, “The influence of thermistor location on temperature measurement from a photonic package,” in *Journal of Physics: Conference Series*, **525**(1), 012004, IOP Publishing (2014).
 - 20 M. Scaggs and G. Haas, “Optical alignment influenced aberrations in laser beam delivery systems and their correction,” in *SPIE LASE*, 93430T–93430T, International Society for Optics and Photonics (2015).